25. Jain, M. K. and Saxena, N. C., Air quality assessment along Dhanbad–Jharia road. *Environ. Monit. Assess.*, 2002, **79**, 239–250.
26. Dubey, B., Pal, A. K. and Singh, G., Trace metal composition of airborne particulate matter in the coal mining and non-mining areas of Dhanbad Region, Jharkhand, India. *Atmos. Pollut. Res.*, 2012, **3**, 238–246.
27. IS 5182, Methods for Measurement of Air Pollution. Part 14, 2000: Guidelines for Planning the Sampling of Atmosphere (Second Revision).
28. Ruzer, L. S. and Harley, N. H., *Aerosols Handbook: Measurement, Dosimetry, and Health Effects*, CRC Press, 2004, 2nd edn, ISBN: 1439855196, 9781439855195, p. 666.
29. GRIMM, *Operation manual of Portable Laser Aerosol spectrometer and dust monitor (Model 1.108/1.109)*, GRIMM Aerosol Technik GmbH & Co. KG, Ainring, Germany, 2010.
30. Peters, T. M., Ott, D. and O'Shaughnessy, P. T., Comparison of the GRIMM 1.108 and 1.109 portable aerosol spectrometer to the TSI 3321 aerodynamic particle sizer for dry particles. *Ann. Occup. Hyg.*, 2006, **50**, 843–850.
31. Grimm, H. and Eatough, D., Aerosol measurement: the use of optical light scattering for the determination of particulate size distribution, and particulate mass, including the semi-volatile fraction. *J. Air Waste Manage. Assoc.*, 2009, **59**(1), 101–107.
32. Burkart, J., Steiner, G., Reischl, G., Moshammer, H., Neuberger, M. and Hitzenberger, R., Characterizing the performance of two optical particle counters (GrimmOPC1.108 and OPC1.109) under urban aerosol conditions. *J. Aerosol Sci.*, 2010, **41**, 953–962.
33. Sastry, V. R., Ram Chandar, K., Nagesha, K. V., Murlidhar, E. and Mohuiddin, M. S., Prediction and analysis of dust dispersion from drilling operation in opencast coal mines. *Procedia Earth Planetary Sci.*, 2015, **11**, 303–311.
34. Jo, W. K. and Park, J. H., Analysis of roadside inhalable particulate matter (PM10) in major Korean cities. *Environ. Manage.*, 2005, **36**, 826–841; doi:10.1007/s00267-004-0341-1.
35. Kumar, P. and Gupta, N. C., Commuter exposure to inhalable, thoracic and alveolic particles in various transportation modes in Delhi. *Sci. Total Environ.*, 2016, **541**, 535–541.
36. Elminir, H. K., Dependence of urban air pollutants on meteorology. *Sci. Total Environ*., 2005, **350**, 225–237.
37. Tiwari, S., Chate, D. M., Pragya, P., Ali, K. and Bisht, D. S., Variations in mass of the PM_{10}, $PM_{2.5}$ and PM_1 during the monsoon and the winter at New Delhi. *Aerosol Air Qual. Res*., 2012, **12**, 20–29.
38. Yadav, S., Praveen, O. D. and Satsangi, P. G., The effect of climate and meteorological changes on particulate matter in Pune, India. *Environ. Monit. Assess.*, 2015, **187**(7), 402; doi:10.1007/s10661-015-4634-z.
39. Brown, J. S., Gordon, T., Price, O. and Asgharian, B., Thoracic and respirable particle definitions for human health risk assessment. *Particle Fibre Toxicol.*, 2013, **10**, 12; http://www.particleandfibretoxicology.com/content/10/1/12
40. Niu, X., Guinot, B., Cao, H. X. and Sun, J., Particle size distribution and air pollution patterns in three urban environments in Xi'an, China. *Environ. Geochem. Health*, 2014, **37**(5), 801–812; doi:10.1007/s10653-014-9661-0.
41. Giuglino, M., Lonati, G., Butelli, P., Romele, L., Tardivo, R. and Grosso, M., Fine particulate ($PM_{2.5}$–PM_1) at urban sites with different traffic exposure. *Atmos. Environ.*, 2005, **39**, 2412–2431.
42. Duzgoren-Aydin, N., Health effects of atmospheric particulates: a medical geology perspective. *J. Environ. Sci. Health C*, 2008, **26**(1), 1–39.
43. Baccini, M., Biggeri, A., Grillo, P., Consonni, D. and Bertazzi, P. A., Health impact assessment of fine particle pollution at the regional level. *Am. J. Epidemiol*., 2011, **174**, 12; doi:10.1093/aje/kwr256.

Received 1 March 2016; revised accepted 1 August 2016

doi: 10.18520/cs/v112/i01/131-139

Nature of suspended particles in hydrothermal plume at 3°40′N Carlsberg Ridge: a comparison with deep oceanic suspended matter

Durbar Ray[1,*], E. V. S. S. K. Babu[2] and L. Surya Prakash[1,3]

[1]CSIR-National Institute of Oceanography, Dona Paula, Goa 403 004, India
[2]CSIR-National Geophysical Research Institute, Uppal Road, Hyderabad 500 007, India
[3]Present address: ESSO-National Centre for Antarctic and Ocean Research, Vasco da Gama, Goa 403 804, India

Suspended matter from hydrothermal plume at 3°40′N Carlsberg Ridge was studied for microtexture and geochemistry. Characteristics of these plume particles were compared with deep-oceanic particulates from different depths. Compared to fine, deep-oceanic suspended matter (≤2.0 μm), some particles in the plume were larger (≥20 μm) and had irregular shape and surface. These plume particles were mostly composed of Fe-oxides and silicates. Bulk composition showed that plume particles were relatively enriched with Fe, P, Mn, rare earth elements (except Ce) and U, but had other trace element concentration analogous to that found in deep-oceanic suspended matter. Efficient scavenging of elements from hydrothermal fluid and sea water makes geochemistry of plume particulates different from common oceanic particles.

Keywords: Deep-oceanic particulates, geochemistry, hydrothermal plume, micro-texture, suspended particulate matter.

BUOYANT hydrothermal fluids emanate from active vents and rise through the water column until it attains neutral buoyancy. During mixing with ambient sea water, dissolved elements in the hydrothermal fluids form metallic sulphides, sulphates, oxides and oxy-hydroxides[1,2]. Commonly, sulphides form at the buoyant stage of any hydrothermal emission, while later oxidation of reduced metals develops oxide particles in non-buoyant plume[3,4]. All these particles of hydrothermal origin are dispersed laterally along with neutrally buoyant plume following deep-sea currents. Such metal-rich hydrothermal particles make major contribution of various trace elements to the oceanic geochemical budget. However, detailed characterization of hydrothermal particles has only rarely been attempted[5].

Recently, hydrothermal plumes from unknown vent(s) were discovered near 3°40′N Carlsberg Ridge[6]. In the present study we determine the morphological and geochemical nature of these plume particles. Geochemistry

*For correspondence. (e-mail: dray@nio.org)

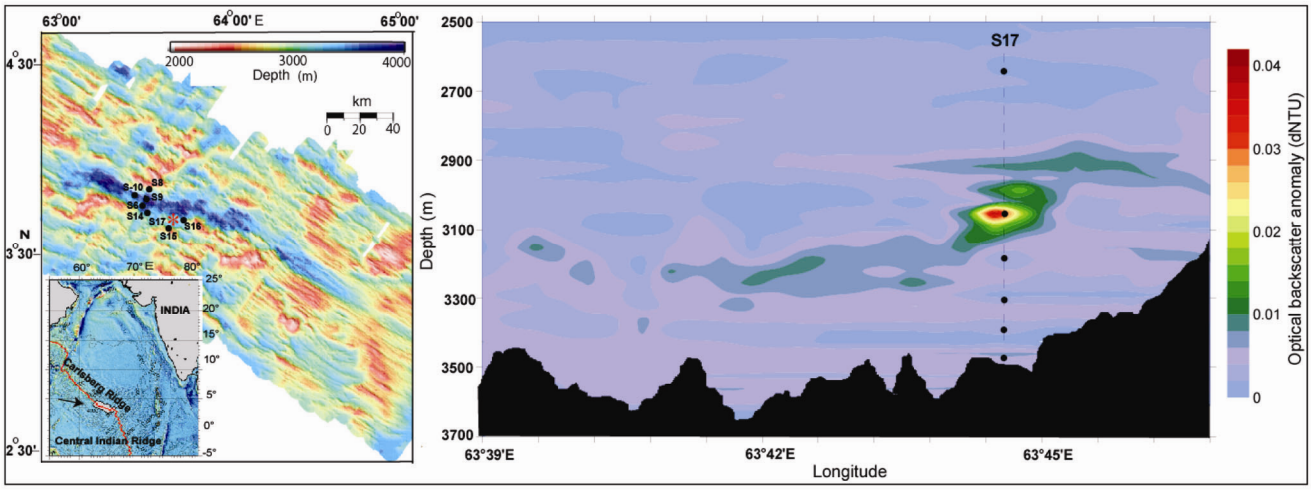

Figure 1. ***a***, Bathymetry of the study area. Red star represents location where intense plume signature has been observed. ***b***, Contour profile of backscatter anomaly indicating turbidity due to dispersal of plume particulates over 3°40′N Carlsberg Ridge[6]. Solid circles represent sampling depths of suspended particulate matter at CTD station S17.

of hydrothermal particulates is compared with common oceanic suspended matter to understand their difference in behaviour in marine environment.

Extending from the southern end of the Owen Fracture Zone near 10°N to the equator in northern Indian Ocean, the Carlsberg Ridge is a typical slow-spreading (11–16 mm/yr) ridge that marks the tectonic plate boundary between the African and Indo-Australian plates[7]. The ridge segment of the present study in the northwestern part is characterized by steep valley wall and wide valley floor. Depth of the rift valley varies between 3000 and 4500 m. Hydrothermal plumes were identified at water depth around 3060 m (ref. 6), near the southwestern wall of the rift valley between 3°40′N and 3°50′N (Figure 1). However, the source locations of active vents have not yet been discovered. Rocks sampled from valley floor and side walls near the plume areas contain mostly fresh basalt with some localized ultramafic outcrops[8].

In order to delineate unknown hydrothermal activities over Carlsberg Ridge, two dedicated expeditions onboard *RV Sonne* (in 2007) and *Akademik Boris Petrov* (in 2009) were carried out for extensive water column studies. During these two cruises, laterally dispersed particle-rich plumes were identified in deep water based on optical anomalies (Figure 1) detected with backscatter sensors of miniature autonomous plume recorders (MAPRs) and conductivity–temperature-depth (CTD) system[6]. The positive temperature anomaly (Figure 2 *a*) at CTD station S-17 (3°40′N, 63°44.8′E) was found to be associated with intense backscatter signature (ΔNTU > 0.01, Figure 2 *b*), excess dissolved ^{3}He (Figure 2 *c*) and manganese (Figure 2 *d*) in water[6], and thus confirming the hydrothermal origin of the plumes.

Deep sea-water was sampled using acid-washed Niskin samplers from the plume layer at 3060 m and a few hundreds of metres above (2600 m) and below (e.g. 3180, 3320, 3400 and 3530 m) the plume. Then 10 litre of each water sample was immediately filtered in duplicate using acid-cleaned, dried 0.45 µm Millipore filter paper (diameter = 47 mm) for textural and geochemical analyses. After filtration, the filters were rinsed thoroughly with Milli-Q water to remove salts from particulate matter. Gentle vacuum was applied for a few minutes using suction pump to remove excess rinsing water. The filter papers were kept in separate petri plates and stored in desiccators until chemical analyses was carried out.

Photomicrographs of suspended matter were examined to visually differentiate particles found in the plume layer and those in other layers in deep sea. Filters with dry particulates were carefully sliced into pieces and fixed on aluminum stubs with glue and then coated with ultra-thin layer of gold using sputtering machine. Particulates on each filter paper were scanned with a JEOL JSM-5410LV scanning electron microscope (SEM). Qualitative chemical composition of selective particles was assessed with an energy dispersive X-ray spectrometer (EDS) attached to the SEM. The operating conditions were generally maintained within the limit of 18 keV, with magnification range from 1000× to 30,000×.

The duplicate sets of filtrates were analysed for bulk elemental composition. In the shore-based laboratory, particulates were digested with ultrapure hydrofluoric acid (3.0 ml), nitric acid (2.0 ml) and perchloric acid (0.5 ml) mixture[9] in acid-washed 30 ml screw-capped teflon vials at 180°C for about 72 h. Completely digested samples were diluted with Milli-Q® water and final volumes were made up to 50 ml. Particulate Fe and Mn concentrations were estimated using a graphite-furnace-AAS (Perkin Elmer Analyst 600), while trace and rare earth elements (REEs) with quadrapole-ICPMS (Thermo

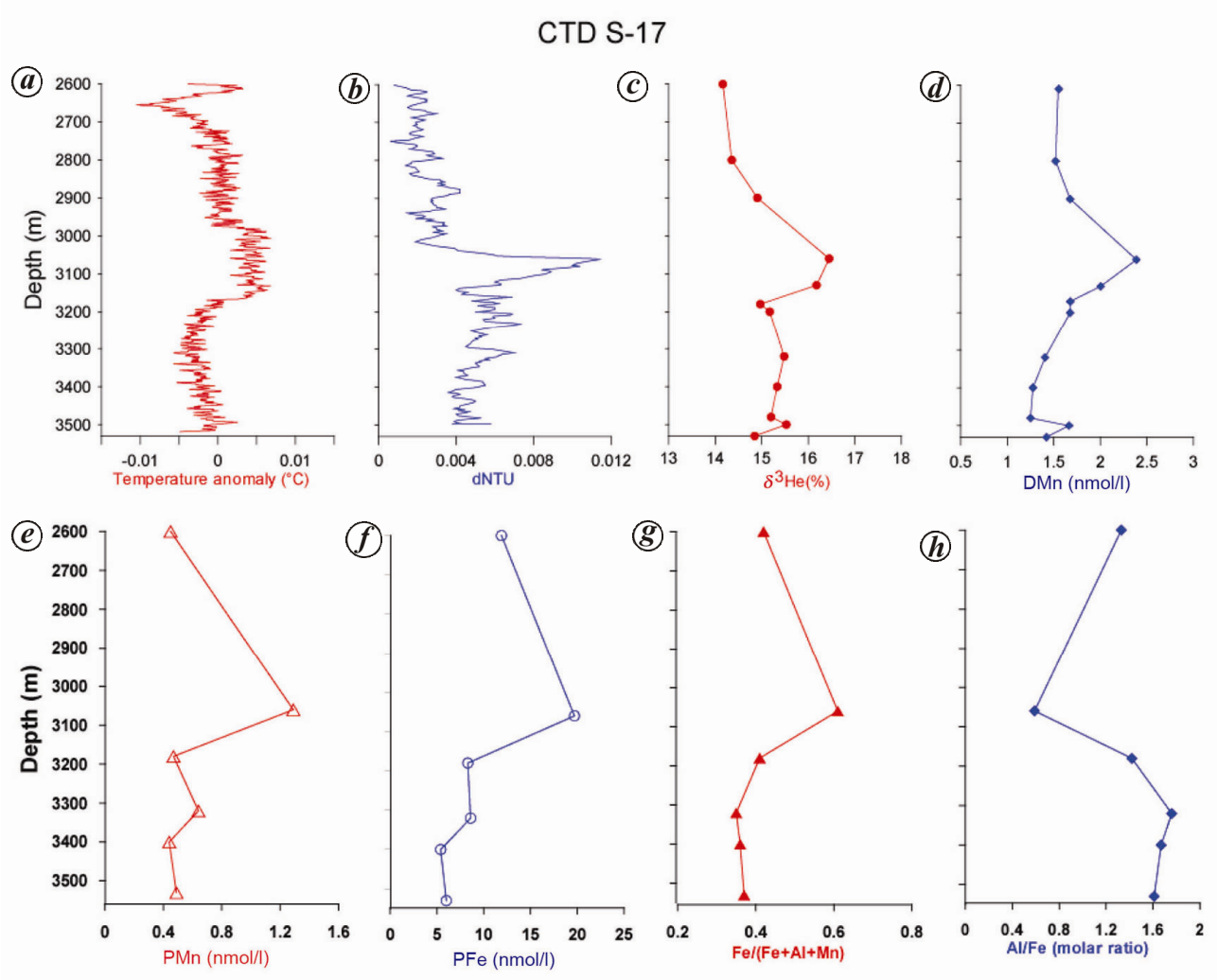

Figure 2. Vertical profiles of (***a***) temperature anomaly, (***b***) backscatter anomaly, (***c***) δ^3He and (***d***) dissolved manganese indicating plume layer[6]. (***e***, ***f***) Anomalous concentrations of particulate manganese (***e***) and iron (***f***) in plume layer. (***g***, ***h***) Profiles of elemental ratio of Fe/(Fe + Al + Mn) (***g***) and Al/Fe (***h***) show anomalous change in plume.

X-Series-II) using ^{103}Rh solution (20 ng/ml) as internal standard. For better signal at extremely low concentration, fine-tuning and optimization of instrumental condition was carried out against aqueous standards. Unused filter papers were digested by similar method and analysed to get the procedural blank values in triplicate. Final results are presented in terms of weight of each element in the particulate filtered from an unit volume of sea water.

In deep water, the observed negligible optical backscatter anomaly (ΔNTU < 0.001) above and below the plume layer indicates very low density of suspended matter. The result also suggests that common suspended matter in deep water column is extremely fine (<2.0 μm). Such fine particles in the deep sea usually contain fine terrigenous minerals, biogenic particles or complex inorganic precipitates[6]. In contrast, particulates from plume-affected nepheloid layer (ΔNTU ~ 0.01 at 3060 m) had a wide size range with numerous larger (>100 μm) particles (Figures 3–5). Some dark large particles were visible to the naked eye. Mixing of hydrothermal fluid with sea water results in the formation of sulphide, sulphate, carbonate and oxide/oxy-hydoxide particles of different sizes (<2.0–~500 μm)[10,11]. Due to high settling velocity, the coarse particles are removed from the plumes immediately after hydrothermal emission[1,11], and thus abundance of larger particles in the dispersed plume, drops sharply as the plume moves away from the source. A model study on plumes over ASHES vent field showed that larger (>100 μm) sulphide/sulphate particles settle very close (<1.0 km) to the active sources[1]. Therefore, large plume particles in the present study perhaps indicate that the unidentified active vent(s) are close to the sampling site. SEM images also show that large plume particles have irregular shape and were characterized by either flaky or platy surface features (Figures 3 and 4). Ray *et*

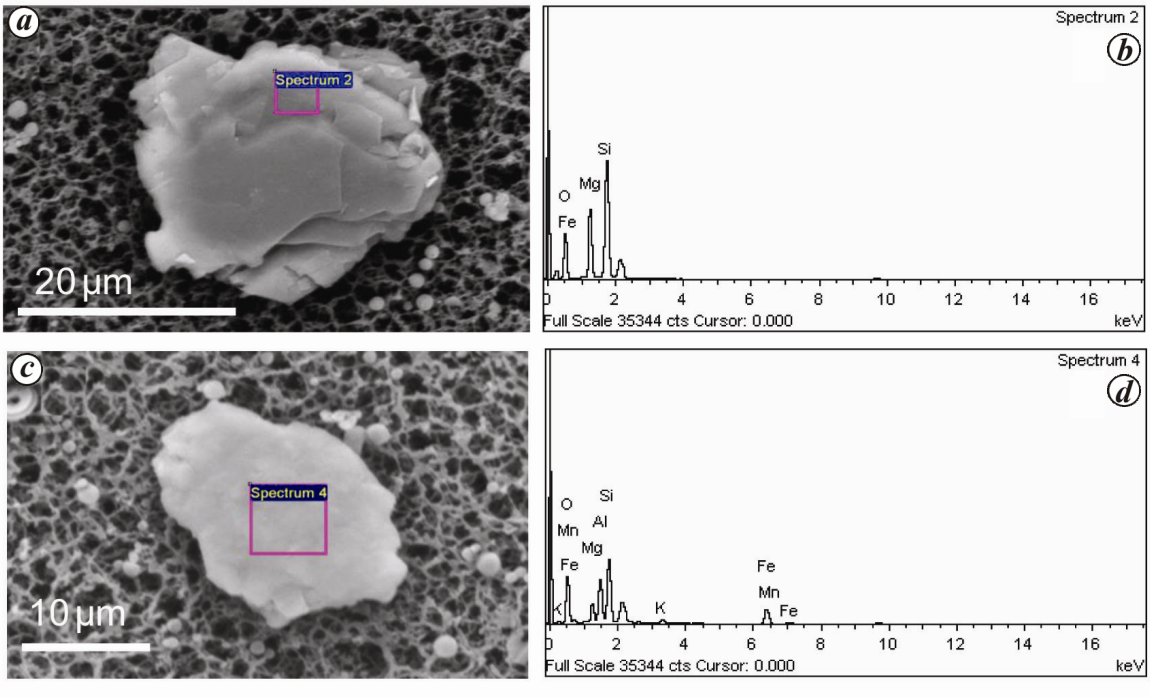

Figure 3. ***a***, ***c***, SEM images of platy Mg–Si-rich plume particles (modified after Ray *et al.*[6]) from 3060 m at station S17; ***b***, ***d***, The corresponding EDS-spectra.

al.[6] showed more images of larger particles (~200 µm) from the same non-buoyant plume over Carlsberg Ridge.

EDS analyses showed that fine circular particles from the plume were mostly composed of siliceous materials, while large particles were enriched in Fe, Mg, Al and Si (Figures 3 and 4). Based on external morphology and elemental composition, three types of large particles are identified: (i) irregular, flaky, Fe-rich, (ii) platy, Mg and Si-rich, and (iii) carbon-containing particles. Following seafloor hydrothermal emission, hydrous metal-oxides having low solubility products can persist within the plume[3] and they grow larger due to aggregation of colloidal particles with time[12]. Therefore, the large, Fe-rich oxides or silicate particles within this nepheloid layer indicate maturity of the plume. Flaky particles are Fe-silicates or Fe-oxides (Figure 4 *a*–*d*) with traces of Ca, Na, K, Al, Mn, Zn and Ti (Figure 4 *e*–*h*). The second type of platy Mg-rich particles had thin-layered texture (Figure 3 *a*–*c*). Based on the elemental ratio, Ray *et al.*[6] proposed that these Mg-silicate particles are talc which is commonly found in ultramafic-hosted hydrothermal systems. EDS analyses of these Mg-rich particles showed the presence of Al and Fe (Figure 3 *d*–*f*) in their siliceous lattice. Ortega-Osorio and Scott[13] have also reported similar Fe-rich, Mg-silicate particles in hydrothermal plumes in the Manus Basin. Some plume particles have very smooth surface with distinct carbon and oxygen peaks in EDS analyses (Figure 5); they are either carbonates or biogenic organic debris adsorbed onto oxide particles. Similar carbon-rich particulates of chemosynthetic origin are also reported in other known hydrothermal plumes[14]. However, none of these large particles was detected with sulphur in EDS analyses; therefore, they are most likely poly-metallic oxides, oxy-hydroxides and silicates, but not sulphides. Absence of large sulphide particles could be due to either ageing of non-buoyant plume or because of high metal-to-H_2S ratio in the parent fluid. Generally, hydrothermal sulphides settle fast within the rising plume as well as beneath the dispersing plumes. Differential sedimentation keeps the larger sulphide and sulphate particles out of the plume immediately after emission[1,4]. Sulphides are also likely to be dissolved, as the non-buoyant plumes mix with the ambient sea water[15,16], and thus might not be available in mature plumes. Therefore, particles from the plume layer differ from suspended matter in normal deep sea water in terms of their physical texture as well as chemical characteristics.

Tables 1 and 2 show bulk chemical composition of suspended matter from different depths. The data show that composition of particulates filtered from turbid plume layer significantly differs from samples at other depths. Different elements show different degrees of enrichment in plume particulates compared to those in normal deep-oceanic suspended matter. This indicates that partitioning behaviour of elements between dissolved and solid phases in hydrothermal plume. Filtered residues from plume contain more particulate Mn (1.29 nmol/l) compared to normal suspended matter in deep-water layers

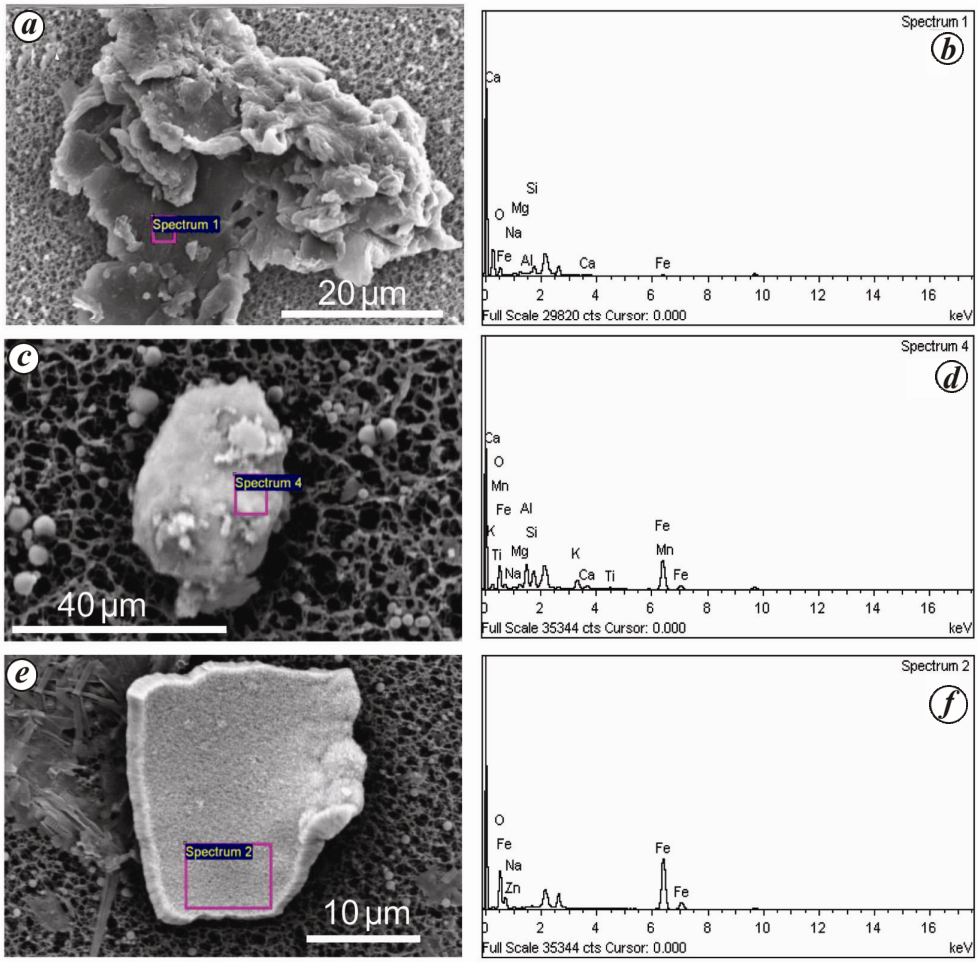

Figure 4. SEM images of (***a***, ***c***) Fe-rich silicates and (***e***) Fe-oxide particles (modified after Ray *et al.*[6]) from the plume at station S17 and (***b***, ***d***, ***f***) their respective EDS-spectra.

Table 1. Trace element composition of suspended particulates from different depths at CTD station S17.

Depth (m)	Mg (µM)	Al (nM)	Ca (nM)	P (nM)	Mn (nM)	Fe (nM)	Zn (nM)	Cu (nM)	Co (pM)	Ni (pM)	Y (pM)	Nb (pM)	U (pM)
2600	0.18	15.8	5.41	15.5	0.45	11.9	1.03	0.39	6.4	112	1.63	0.27	0.29
3060	0.22	11.6	6.99	28.3	1.29	19.7	0.67	0.59	15.6	97.3	3.82	0.65	0.55
3180	0.16	11.7	5.15	16.3	0.47	8.3	1.15	0.52	11.8	NA	2.53	0.16	0.38
3320	0.19	15.1	6.24	11.2	0.64	8.6	0.79	0.5	9.2	71.3	1.97	0.11	0.23
3400	0.19	9.1	6.7	15.7	0.44	5.4	0.93	0.52	6.7	86.8	2.02	0.05	0.23
3530	0.2	9.6	6.59	11.9	0.49	6.0	1.11	0.53	11.3	94.6	1.97	0.27	0.27

(0.4–0.6 nmol/l; Figure 2 *e* and Table 1) above and below the plume.

Concentration of particulate Mn is similar to that reported in Gorda Ridge plumes (0.76–1.66 nmol/l)[3], but higher than Carlsberg event plume (0.46 nmol/l)[9] or Rainbow plume particulates (<0.5 nmol/l)[4]. Dissolved Mn in hydrothermal plume behaves conservatively and hardly any particulate Mn (<20% of total Mn) develops in buoyant plume over active vent source. In the present study, about 35% of total Mn present in particulate phase indicating significant ageing of the plume. Plume particulates composed of large number of Fe-rich silicate and oxide particles, have Fe concentration of ~20 nmol/l (Figure 2 *f*), comparable to non-buoyant plume particulates over Rainbow field (5.7–420 nmol/l)[4]. The background particulate Fe concentration varies between 5.0 and 12 nmol/l in this water column (Table 1). The plume particulates have marginally higher Al (11.6 nmol/l) than those reported in other hydrothermal plumes[2,4], but do not differ much from non-plume samples (9–15 nmol/l) at

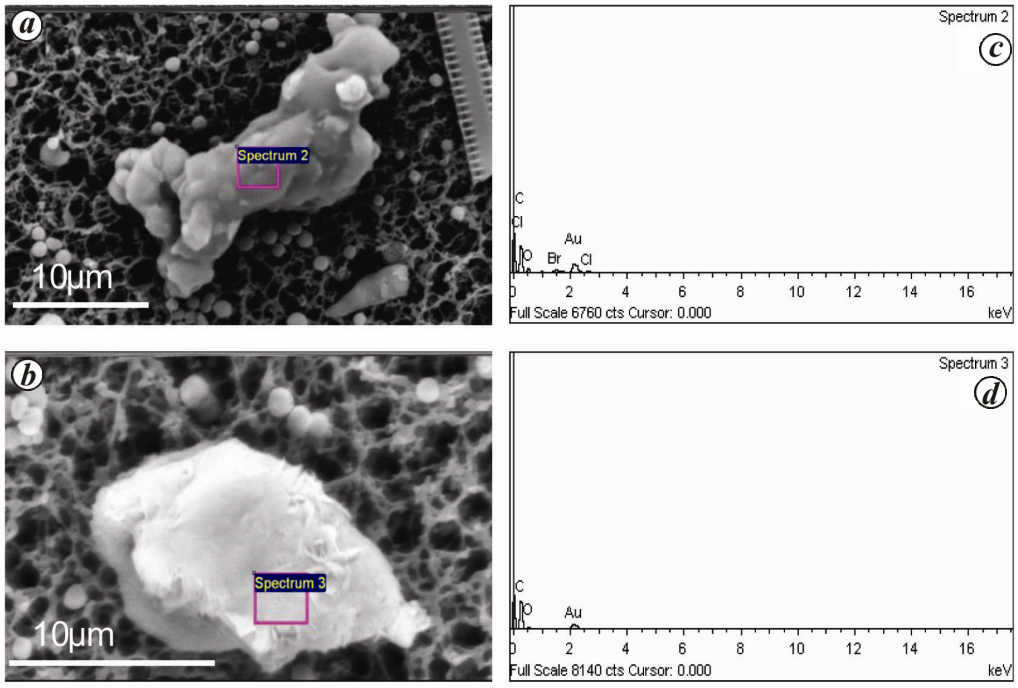

Figure 5. ***a***, ***b***, SEM images of organic particles in suspended particulates from plume (3060 m) at station S17; ***c***, ***d***, their corresponding EDS-spectra.

Table 2. Rare earth element (REE) composition of suspended particulates from different depths at CTD station S17

Depth (m)	La (pM)	Ce (pM)	Pr (pM)	Nd (pM)	Sm (pM)	Eu (pM)	Gd (pM)	Tb (pM)	Dy (pM)	Ho (pM)	Er (pM)	Tm (pM)	Yb (pM)	Lu (pM)
2600	0.88	1.75	0.142	0.805	0.170	0.049	0.182	0.035	0.123	0.030	0.090	BDL	0.087	BDL
3060	1.56	1.64	0.355	1.592	0.340	0.098	0.398	0.063	0.307	0.061	0.211	0.030	0.145	0.023
3180	0.95	1.61	0.177	0.908	0.238	0.065	0.223	0.031	0.184	0.039	0.120	0.018	0.116	0.029
3320	1.74	2.57	0.213	0.839	0.204	0.062	0.252	0.031	0.163	0.036	0.090	0.000	0.087	0.029
3530	0.95	1.88	0.195	0.805	0.170	0.059	0.236	0.038	0.138	0.030	0.090	0.015	0.087	0.020

BDL, Below detection limit.

other depths (Table 1). Slightly low concentration of particulate Al in deeper waters confirms that there is no input of Al due to re-suspension of bottom sediment, as found in sedimented ridge segments[2]. Al-to-Fe ratio is notably low (Al/Fe = 0.59, Figure 2 *h*) within the plume compared to other samples (Al/Fe > 1.3). More than 50% drop in Al-to-Fe ratio at 3060 m is not likely due to change in water mass with depth. The enrichment of Fe relative to Al in suspended particulates indicates more hydrothermal than detrital input[4]. The reverse trend of Al/Fe ratio in the rest of the water column appears to be due to dry deposition of dust and other terrigenous sources. The maximum enrichment of particulate Fe (Fe/(Fe + Mn + Al) > 0.6, Figure 2 *g*) and relative depletion of particulate Al (Al/Fe < 0.59, Figure 2 *h*), therefore indicate hydrothermal contribution in the sample from 3060 m.

Mg and Ca, two complementary elements, did not show significant difference between plume particulate and normal deep-oceanic particles from other depths. Marginal changes in Mg (0.16–0.22 µmol/l) and Ca (5.1–6.9 nmol/l) in the plume suggest negligible role of hydrothermal contribution on the concentration of these two elements. Otherwise, during mixing with seawater, Mg and Ca in the fluid commonly precipitate as hydroxide, sulphate or silicates. As described earlier, minute salt particles in the suspension, possibly cause minor increase of these elements in particulate phase of the plume layer and also support the existence of Mg–silicate minerals in the plume layer. Chalcophiles like Cu, Zn and Ni did not show significant change in the neutrally buoyant plume particles (Table 1). These elements of hydrothermal origin precipitate mostly as sulphides near the active vent source. Therefore, lack of excess chalcophile elements in this nephloid layer suggests that the plume has been diluted at the sampling site S17. In contrast, distribution of particulate phosphorus in the water column showed considerable enrichment within the plume (28 nmol/l)

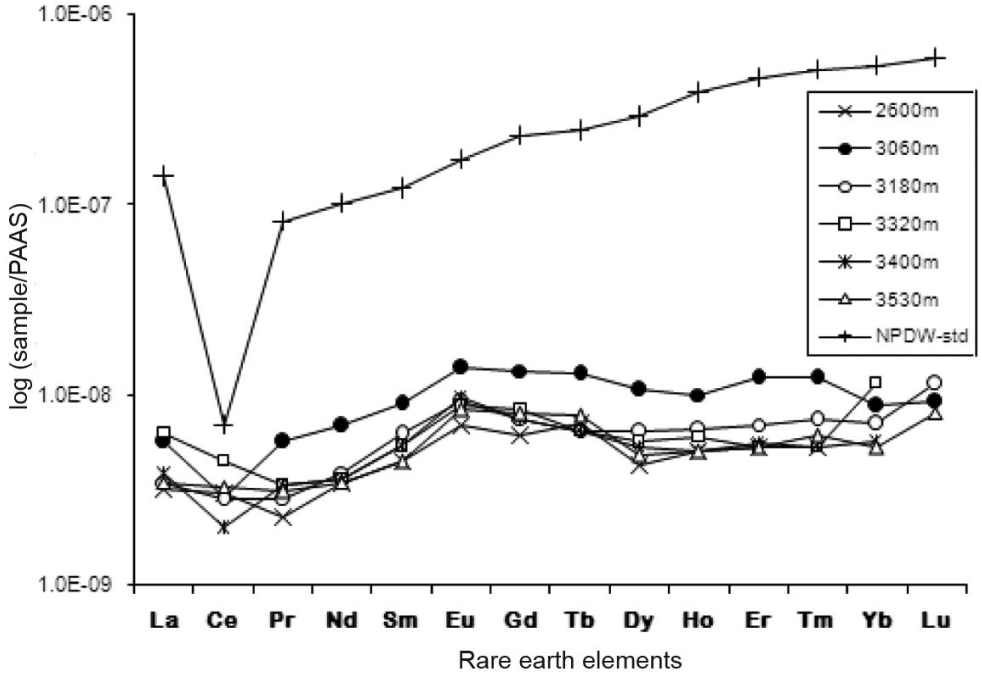

Figure 6. Shale-normalized REE patterns for suspended particulates filtered from different depths. Solid circles indicate plume sample from 3060 m.

Table 3. Geochemical characteristics of trace and REEs in suspended particulates from different depths at CTD station S17

Depth (m)	Mn/Fe (nM/nM)	Fe/(Fe + Al + Mn) (nM/nM)	Al/Fe (nM/nM)	P/Fe (nM/nM)	Ce/Ce*	Nd_n/Yb_n
2600	0.038	0.42	1.33	1.31	1.06	0.65
3060	0.065	0.61	0.59	0.83	0.51	0.77
3180	0.057	0.41	1.42	3.41	0.87	0.55
3320	0.075	0.35	1.76	1.31	0.84	0.68
3530	0.082	0.37	1.61	1.99	0.98	0.65

relative to background concentration (11–15 nmol/l, Table 1). Phosphorus usually exists as dissolved phosphate in sea water and has the affinity to be adsorbed on positively charged colloidal Fe-oxy-hydroxide particles. Thus scavenging of P from sea water by nascent Fe-oxide-rich plume particles appears to be responsible for increase of particulate P in the plume layer. Similar enrichment of oxy-anions of P, V, Cr and As in hydrothermal plume particles has also reported in EPR, Cleft and Rainbow vent fields[4,17]. Relatively high concentration of heavy elements like uranium (0.55 pmol/l) in the plume layer is probably due to scavenging of U(VI) from ambient sea water. Redox-sensitive U quantitatively precipitates from sea water during hydrothermal mixing[18], as dissolved U(VI) converts into insoluble U(IV)-oxides.

Most of the REEs have slightly higher concentrations in the plume layer (at 3060 m) relative to other depths (Table 2). Yttrium, which is considered as pseudo-lanthanide, also has higher concentration in plume particles (3.8 pmol/l) compared to samples from other depths (1.6–2.6 pmol/l) (Table 2). Enrichment of REEs in plume-derived particles could be due to preferential adsorption and co-precipitation of particle-reactive non-conservative REE species from sea water (and hydrothermal fluid). Particularly, Fe-rich metal-oxide/oxy-hydroxide in suspended particulate matter (SPM) of hydrothermal origin is reported to sorb dissolved REE more effectively[19]. Irregular shape and larger surface area possibly enhance such scavenging capacity in hydrothermal particles. Shale (PAAS) normalized REE patterns of SPM from 3060 m also differ from the rest (Figure 6) and indicates that except for Ce, partitioning of REEs with respect to sea water differs in hydrothermal plume particulates.

It is interesting to note that relative fractionation between light and heavy REEs in plume particulates ($Nd_n/Yb_n = 0.8$) (Table 3) is close to that observed in SPM from other depths ($Nd_n/Yb_n = 0.6–0.72$) (Table 3), or typical deep-oceanic hydrogenous particles[5]. No

prominent positive Eu anomaly, a common character of hydrothermal plumes, was found in shale-normalized pattern of plume particulates. These results suggest that plume dispersal at 3060 m was mature and had been extremely diluted with sea water. Even though the plume was diluted at the sampling site, significant negative Ce anomaly (Ce/Ce* = 0.5) (Table 3) in plume particulates differs from those at other depths (Ce/Ce* = 0.84–1.06; Table 3). During mixing with sea water dissolved Ce(III) of hydrothermal origin prefers to remain in solution phase rather than in solid hydrothermal particulates. Similar behaviour of redox-sensitive Ce has been reported in non-buoyant plume particulates over TAG[20] and Rainbow[4] vent fields. In contrast, hydrogenous particulates have very weak or no Ce anomaly, indicating sufficient scavenging of Ce(IV) from oxygen-rich deep waters.

The particulate matter of hydrothermal plume at 3°40′N Carlsberg Ridge was found to have a range of sizes with a variety of textures and distinctly differed from fine suspended matter in the deep sea. The elevated concentrations of trace elements in particulates of this non-bouyant plume resemble typical high-temperature plumes of other vent fields. During hydrothermal fluid–sea-water mixing, co-precipitation and scavenging enhance the trace element concentrations in plume particulates. Thus geochemical characters of particulates suggest that the Carlsberg plume originates from high-temperature vent fluid. Further surveys are required to locate the active unknown vent(s) along this ridge segment.

1. Feely, R. A., Geiselman, T. L., Baker, E. T., Massoth, G. J. and Hammond, S. R., Distribution and composition of buoyant and non-buoyant hydrothermal plume particles from the ASHES vent at Axial Volcano, Juan de Fuca Ridge. *J. Geophys. Res*., 1990, **95**, 12855–12874.
2. Feely, R. A., Massoth, G. J., Trefry, J. H., Baker, E. T., Paulson, A. J. and Lebon, G. T., Composition and sedimentation of hydrothermal plume particles from North Cleft segment, Juan de Fuca Ridge. *J. Geophys. Res*., 1994, **99**, 4985–5006.
3. Feely, R. A., Baker, E. T., Lebon, G. T., Gendron, J. F., Massoth, G. J. and Mordy, C. W., Chemical variations of hydrothermal particles in the 1996 Gorda Ridge Event and chronic plumes. *Deep-Sea Res. II*, 1998, **45**, 2637–2664.
4. Edmond, H. N. and German, C. R., Particle geochemistry of Rainbow hydrothermal plume; Mid-Atlantic Ridge. *Geochim. Cosmochim. Acta*, 2004, **68**, 759–772.
5. Lerche, D. and Nozaki, Y., Rare earth elements of sinking particulate matter in the Japan Trench. *Earth Planet. Sci. Lett*., 1998, **159**, 71–86.
6. Ray, D. *et al.*, Hydrothermal plumes over the Carlsberg Ridge, Indian Ocean. *Geochem. Geophys. Geosyst*., 2012, **13**; doi: 10.1029/2011GC003888.
7. Merkouriev, S. A. and Sotchevanova, N. A., Structure and evolution of the Carlsberg Ridge: evidence for non-stationary spreading on old and modern spreading centres. *Curr. Sci*., 2003, **85**, 334–338.
8. Mudholkar, A. V., Kodagali, V. N., Kamesh Raju, K. A., Valsangkar, A. B., Ranade, G. H. and Ambre, N. V., Geomorphological and petrological observations along a segment of slow-spreading Carlsberg Ridge. *Curr. Sci*., 2002, **82**, 982–989.
9. Ray, D. *et al.*, Water column geochemical anomalies of remnant of a mega plume: a case study after CR-2003 hydrothermal event in Carlsberg Ridge, NW Indian Ocean. *Curr. Sci.*, 2008, **95**, 355–360.
10. Dymond, J. and Roth, S. E., Plume dispersed hydrothermal particles: a time-series record of settling flux from the Endeavor Ridge using moored sensors. *Geochim. Cosmochim. Acta*, 1988, **52**, 2525–2536.
11. German, C. R. and Sparks, R. S. J., Particle recycling in TAG hydrothermal plume. *Earth Planet. Sci. Lett.*, 1993, **116**, 129–134.
12. Massoth, G. J. *et al.*, Manganese and iron in hydrothermal plumes resulting from the 1996 Gorda Ridge Event. *Deep-Sea Res. II*, 1998, **45**, 2683–2712.
13. Ortega-Osorio, A. and Scott, S. D., Morphological and chemical characterization of neutrally buoyant plume-derived particles at the eastern Manus basin hydrothermal field. *Can. Miner.*, 2001, **39**, 17–31.
14. Roth, S. E. and Dymond, J., Transport and settling of organic material in a deep-sea hydrothermal plume: evidence from particle flux measurements. *Deep-Sea Res. I*, 1989, **36**, 1237–1254.
15. German, C. R., Klinkhammer, G., Edmond, J. M., Mitra, A. and Elderfield, H., Hydrothermal scavenging of rare-earth elements in the ocean. *Nature*, 1990, **345**, 516–518.
16. Feely, R. A., Massoth, G. J., Baker, E. T., Lebon, G. T. and Geiselman, T. L., Tracking the dispersal of hydrothermal plumes from the Juan de Fuca Ridge using suspended matter compositions. *J. Geophys. Res*., 1992, **97**, 3457–3468.
17. Trefry, J. H., Trocine, R. P., Klinkhammer, G. P. and Rona, P. A., Iron and copper enrichment of suspended particles in dispersed hydrothermal plume along the Mid-Atlantic Ridge. *Geophys. Res. Lett*., 1985, **12,** 506–509.
18. Chen, J. H., Wasserburg, G. J., Von Damm, K. L. and Edmond, J. M., The U–Th–Pb systematics in hot springs on the East Pacific Rise at 21°N and Guaymas Basin. *Geochim. Cosmochim. Acta*, 1986, **50**, 2467–2479.
19. Mitra, A., Elderfield, H. and Greaves, M. J., Rare earth elements in submarine hydrothermal fluids and plumes from the Mid-Atlantic ridge. *Mar. Chem*., 1994, **46**, 217–235.
20. Rona, P. A., Klinkhammer, G., Nelsen, T. A., Trefry, J. H. and Elderfield, H., Black smokers, massive sulfides and vent biota at the Mid-Atlantic Ridge. *Nature*, 1986, **321**, 33–37.

ACKNOWLEDGEMENTS. We thank the Directors, CSIR-NIO, Goa and CSIR-NGRI, Hyderabad for their encouragement and the masters and crew of *RV Sonne* and *Akademik Boris Petrov* for their support. This study was funded by MoES project, GAP-2157, CSIR projects, PSC-0106 (GEOSINKS) and PSC-0204. We also thank V. D. Khedekar for SEM-EDS analysis, and the three anonymous reviewers for their valuable comments. This is NIO contribution number 5930.

Received 9 May 2015; revised accepted 8 August 2016

doi: 10.18520/cs/v112/i01/139-146